Superlattices and Microstructures 60 (2013) 426–436

Contents lists available at SciVerse ScienceDirect

Superlattices and Microstructures

journal homepage: www.elsevier.com/locate/superlattices

Enhancement mechanism of photovoltaic performance for ZnO/CdS heterostructure photoelectrodes via post-annealing treatment

Lili Yang [a,b,c], Zhiqiang Zhang [a,c], Jinghai Yang [a,c,*], Yongsheng Yan [b], Yunfei Sun [d], Guangbo Che [c], Zhe Wang [a,c], Shi Zhang [c]

[a] Institute of Condensed State Physics, Jilin Normal University, Siping 136000, People's Republic of China
[b] Institute of Chemistry and Chemical Engineering, Jiangsu University, Zhenjiang 212013, People's Republic of China
[c] Key Laboratory of Functional Materials Physics and Chemistry, Jilin Normal University, Ministry of Education, Siping 136000, People's Republic of China
[d] Key Laboratory of Excited State Physics, Changchun Institute of Optics Fine Mechanics and Physics, Chinese Academy of Sciences, Changchun 130033, People's Republic of China

ARTICLE INFO

Article history:
Received 15 January 2013
Received in revised form 19 April 2013
Accepted 20 May 2013
Available online 29 May 2013

Keywords:
ZnO nanorods
Cadmium sulfide quantum dots
Post-annealing treatment
Energy conversion efficiency

ABSTRACT

High-density and vertically-aligned cadmium sulfide quantum dots (CdS QDs) sensitized Zinc oxide nanorods (ZNRs) heterostructure as photoelectrode had been used to fabricate the quantum dots sensitized solar cells. The effect of post-annealing temperature was investigated on their photovoltaic performance. The power conversion efficiency was improved significantly after annealing treatment, which can be attributed to two factors: on the one hand, the increase in grain size of CdS quantum dots after annealing results in the enhancement of absorption intensity and expansion of absorption spectral range; on the other hand, the post annealing treatment can reduce the defect concentration and highly improve the crystallization quality of the ZNRs/CdS photoelectrodes. The highest power conversion efficiency of the solar cell can achieve 1.14% with a J_{SC} of 5.27 mA/cm^2 and a V_{OC} of 0.51 V under the white light illumination intensity of 100 mW/cm^2.

* Corresponding author at: Institute of Condensed State Physics, Jilin Normal University, Siping 136000, People's Republic of China. Tel.: +86 434 3290009; fax: +86 434 3294566.
E-mail address: jhyang1@jlnu.edu.cn (J. Yang).

0749-6036/$ - see front matter © 2013 Elsevier Ltd. All rights reserved.
http://dx.doi.org/10.1016/j.spmi.2013.05.025

1. Introduction

Quantum dot sensitized solar cells (QDSSCs) are gaining renewed attention throughout the world from both academic and industrial fields, due to their simple fabrication procedure and low cost manufacturing possibilities [1]. Semiconductor quantum dots (QDs) light harvesting elements can replace organic dyes in a typical dye sensitized solar cell structure as it has a higher absorption coefficient compared to organic dye molecules [2], long-term photostability [3], tunable size-bandgap property [4], multiple exciton generation capability through impact ionization [5]. which has potential to boost QD solar cell power conversion efficiencies higher than the conventional silicon based solar cell commercially available today [5,6]. Among the various semiconductor QDs, such as CdS, CdSe, CdTe and PbS, used in QDSSCs, cadmium sulfide (CdS) is one of the most widely used material due to its bulk bandgap of 2.42 eV and direct bandgap absorption characteristics [7]. Several reports on CdS QDSSCs mostly using titanium dioxide (TiO_2) as photoelectrode material have been reported till date [8–10]. And the highest efficiency recorded by TiO_2 QDSSCs has reached 4.81% due to the electron transport and electron collection efficiency has been improved by the CdSe/CdS cosensitized solar cell [11].

Zinc oxide (ZnO) is one of the most extensively studied materials as an alternative photoanode to TiO_2, since it has a direct bandgap, higher exciton energy, and higher electron mobility and can be grown in various shapes with relative ease [1]. In particular, its 1D nanostructure arrays can be grown easily over a large area on different substrates by a variety of methods. The array configuration of ZnO nanostructures could enhance light absorption due to scattering and trapping, which may also benefit their photovoltaic applications [12,13]. In addition, ZnO nanorods could provide a direct current pathway for electrons to the external circuit with few grain boundaries [14]. Recently, QDSSCs based on CdS sensitized ZnO nanorod arrays have been variously studied. Han et al. reported 0.54% photovoltaic performance based on CdS QDs sensitized ZnO nanorod arrays [15]. Wang et al. also fabricated ZnO nanorod arrays/CdS QDs heterogeneous films and obtained a conversion efficiency of 0.34% [16]. Thus, the conversion efficiency of CdS QDSSC using ZnO nanorods as photoelectrode material is still relatively low (less than 0.6%) in the above literatures. To improve the assembly techniques of the solar cells is an effective way to enhance the solar energy conversion efficiency of final devices. The post-thermal annealing treatment is one of the well-suitable methods. On one hand, the as-deposited films usually have poor crystallinity, thus, the thermal annealing treatment can effectively improve their quality [17,18]. On the other hand, it is also possible to enhance the photovoltaic performance by optimizing the photoelectrode through the thermal annealing treatments process, which could reduce the concentration of defects obviously, and could improve the electric transport property of both quantum dots and photoanode [19,20]. However, up to now, few investigations have been reported about the CdS QDs sensitized ZnO nanorod arrays photoanode, especially for the detailed mechanism of photovoltaic properties, which is really urgent to be studied due to the promising significant contribution for development of CdS sensitized ZnO nanorod arrays photovoltaic devices.

In this work, we present a type of QDSSCs with CdS quantum dots adsorbed on ZNRs to convert light into electrical current flow. The effect of post-annealing temperature and the way of post-annealing on the photovoltaic performance of ZNRs/CdS photoelectrodes on the structure, optical properties, and photovoltaic performances of the device have been investigated in detail for the first time to our best knowledge, which help us to reveal the enhancement mechanism of energy conversion efficiency. This study not only demonstrates the enhanced photovoltaic performance of ZNRs/CdS due to a controlled annealing but also gives some insights about the fundamental mechanisms that promote the improvement.

2. Experimental details

2.1. Preparation of vertically aligned ZNRs

The ZNRs were grown on indium tin oxide (ITO) substrates by the chemical bath deposition (CBD) method, which includes a two-step process, i.e., a substrate treatment prior to the CBD growth. The pretreatment of the substrates, by coating the substrate for different times with a 2.5 mM solution

of zinc acetate dihydrate ($Zn(OOCCH_3)_2{\cdot}2H_2O$, 99.9% purity) dissolved in pure ethanol. This solution was coated three times onto ITO substrates by a spin coater (LaurellWS-400-8TFW-Full) at the rate of 2000 rpm for 30 s, and then the ITO substrate with a seed layer was annealed at 300 °C for 1 h. In the CBD growth, the precursor aqueous solution composed of 0.1 M aqueous solutions of zinc nitrate hexahydrate ($Zn(NO_3)_2{\cdot}6H_2O$, 99.9% purity) and 0.1 M aqueous solutions of methenamine ($C_6H_{12}N_4$, 99.9% purity) in a 1:1 M ratio were first prepared and mixed together. The pretreated ITO substrates were immersed into the aqueous solution with sealing the beaker, which was placed in a regular laboratory oven and heated to 95 °C for 5 h. After growth, the samples were washed by deionized water for several times and dried at room temperature.

2.2. Deposition of CdS QDs

The CdS QDs was deposited on the crystallized ZNRs by a successive ionic layer adsorption and reaction (SILAR) technique. Typically, the samples of ZNRs were successively dipped in two different aqueous solutions for 5 min. One is containing Cd^{2+} cations (0.2 M $Cd(NO_3)_2$) and the other is containing S^{2-} anions (0.2 M Na_2S). Between each immersion step, the samples were rinsed with de-ionized water for 30 s to remove excess ions that were weakly bound to the samples surfaces. The two-step dipping procedure is termed as one SILAR cycle. The incorporated amount of CdS can be increased by repeating the assembly cycle. After several cycles, the color of samples turned into yellow. Subsequently, the samples were thoroughly washed with ethanol and deionized water and then dried at room temperature. It is well known that the performance of QDSSCs depend on the SLIAR cycles for depositing QDs to sensitize ZnO film. The effect of SLIAR cycles on the device performance has been carefully studied. We find that the optimum number of SILAR cycles for CdS is about six. Therefore, in our experiment, we used six cycles to deposit CdS QDs on the ZNRs samples. The post-thermal annealing processes were performed in an open horizontal tubular furnace at different temperatures (200, 300, 400, 500 °C) for 1 h. The names corresponding to each cell annealed at different temperature are shown in Table 1. Besides the above samples, we have synthetized the other one by changing the annealing process. The fabrication process is as follows: after the three SLIAR cycles of CdS QDs deposition on the surface of ZNRs, the sample is post-annealed at 400 °C for 1 h. Then, another three SLIAR cycles of CdS QDs deposition is performed on the sample. Thus, the sample was named 3N/3A4.

2.3. QDSSCs assembly

The CdS QDs sensitized ZNRs electrode was incorporated into thin-layer sandwich-type cells. A 20 nm platinum-sputtered ITO substrate as the counter electrode and the working electrode were positioned face-to-face. The iodide-based electrolyte, consisting of 1 M LiI and 0.05 M I_2 in alcohol, was injected into the interelectrode space by capillary action.

2.4. Characterization of samples

The scanning electron microscope (SEM, S-570, Hitachi) with an energy dispersive X-ray analysis (EDAX) spectroscopy system was used to evaluate the morphology and elemental composition of the samples. The transmission electron microscope (TEM, JEM-2100, JEOL) with an energy dispersive X-ray analysis (EDAX) spectroscopy system was used to qualitatively confirm the detailed microscopic

Table 1
The number of SILAR cycles and annealing temperature for each sample.

Samples name	SILAR cycles	Annealing temperature
N	6	As-deposition
A2	6	200 °C
A3	6	300 °C
A4	6	400 °C
A5	6	500 °C

structure and different chemical composition of the samples. The photoluminescence (PL) measurements were performed on the Renishaw invia spectroscopy excited by a continuous He–Cd laser with a wavelength of 325 nm at a power of 2 mW. The Ultraviolet–visible (UV–vis) absorption spectra of each photoelectrode were recorded on a UV–vis spectrophotometer (UV-5800PC, Shanghai Metash Instruments Co., Ltd.) at room temperature. The photocurrent dependence on the voltage (*I–V*) were measured under AM 1.5G simulated sunlight illumination (100 mW/cm^2, Model 91160, Oriel).

3. Results and discussion

Fig. 1a and b shows the morphology of ZNRs before and after CdS deposition. Fig. 1a shows the typical SEM image of the as-grown ZNRs. It can be seen that the vertically-aligned ZNRs with ~150 nm diameter uniformly cover the entire ITO substrate with high density. All of ZNRs show hexagonal faceted and smooth surfaces. Fig. 1b is the SEM image of N sample, i.e. ZNRs with deposition of CdS. The morphology of ZNRs retained their constant, but the roughened texture of surface is clearly visible. We can observe that a number of small nanoparticles attached on the surface of ZNRs and the diameters of the ZNRs tips increased in comparison with Fig. 1a. The inset of Fig. 1a and b shows the photo image for ZNRs and N samples. After sensitizing CdS QDs, the color of sample changed from white to yellow. Hence, we can deduce that CdS QDs have been successfully deposited onto the surface of the ZNRs, which will be further confirmed by TEM analysis below. In order to verify the CdS QDs elemental composition, we further performed EDAX measurement on the ZNRs sensitized with CdS QDs (inset of Fig. 1b). The characteristic peaks in the spectrum can be identified to the Zn, O, Cd and S elements. Their corresponding quantitative concentration has been estimated to be 47.53%, 45.87%, 3.43%, and 3.17%, respectively. Moreover, quantitative analysis of the EDAX spectrum reveals that the molar ratio of Cd to S is close to 1:1, further confirming the stoichiometric formation of CdS on ZNRs. These results indicate that CdS QDs have been successfully assembled onto the surface of the ZNRs.

After the as-deposited N samples were obtained by SILAR technique, they were post-annealed in air for 1 h at different temperatures (200, 300, 400, 500 °C). Fig. 1c–f shows the morphology evolution of the as-deposited N with different post-annealing temperatures. In comparison with the surface of as-deposited N sample in Fig. 1b, we can find that with increasing the post-annealing temperature, the surface turned smoother and smoother, as shown in Fig. 1c–e. It is interesting to note that post-annealing at 400 °C result in a continuous shell morphology of CdS layer for A4 sample instead of nanoparticles morphology in sample of A2 and A3. As a result of CdS grain growth and migration, the ZNRs are fully covered by CdS, which inhibit the charge recombination of percolated electrons in the ZNRs and oxidizing species in the electrolyte. Thus the thermal annealing treatments process could effectively promote the charge collection and reduce the recombination losses between the bare ZNRs and electrolyte, which produces better photovoltaic performances than the as-deposited ZNRs/CdS. The migration observed in Fig. 1e points out that matter transport, which is a hardly expected phenomenon in completely solid systems, takes place during thermal annealing at 400 °C for as-deposited N samples. This could be easily promoted by the beginning of a CdS liquid phase (likely in surface), suggesting a dramatic decrease of the melting point of CdS shell with respect to bulk material. A similar decrease in melting temperature was previously reported in CdS nanocrystals [21,22]. With increasing the annealing temperature to 500 °C, the sample shows hexagonal faceted and smooth surfaces, as shown in Fig. 1f, which is quite similar to the morphology of ZNRs in Fig. 1a. Meanwhile, the color of ZNRs/CdS film change from yellow to white, which implies the disappearance of CdS on the ZNRs surface. To prove this deduction, we take the EDAX measurement for A5. As shown in the inset of Fig. 1f, only the characteristic peaks of Zn and O elements were detected in A5 (inset of Fig. 1f). This is because that the S and Cd atoms evaporate from the film at 500 °C, resulting in a disappearance of CdS films [17].

The further detailed microscopic structure of N and A4 samples were characterized by TEM. Fig. 2a and b presents the TEM images of N and A4, respectively, which clearly shows that the average diameter of two samples is ~150 nm. Fig. 2a is the TEM image of a single ZNR with loading CdS QDs for six cycles. We can observe that a layer of ultrafine nanoparticles as the circular dark spots uniformly

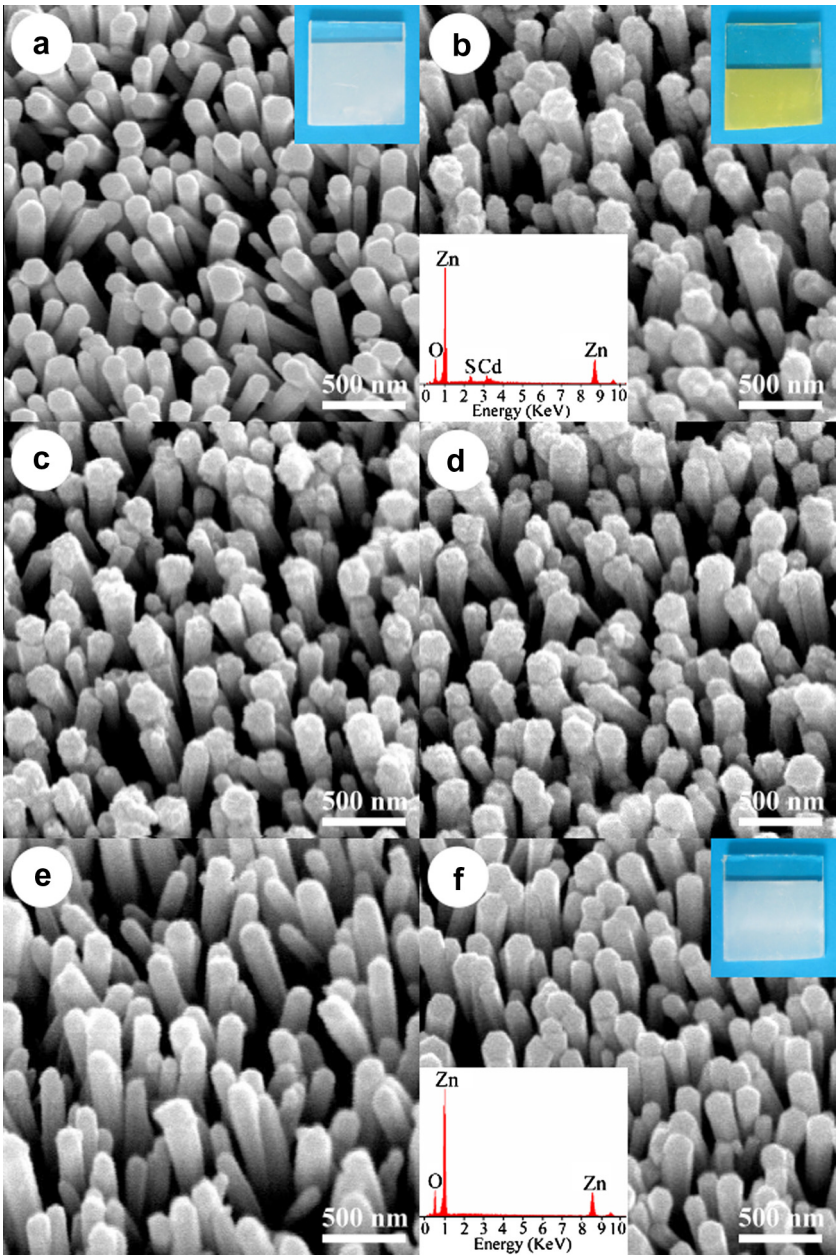

Fig. 1. SEM images of large-scale dense arrays of well-aligned (a) ZNRs and (b) N grown on ITO glass substrate (inset: EDAX). SEM images of N after different annealing temperatures: (c) A2 (annealing temperature: 200 °C), (d) A3 (annealing temperature: 300 °C), (e) A4 (annealing temperature: 400 °C) and (f) A5 (annealing temperature: 500 °C) (inset: EDAX). The inset shows the photo image for ZNRs, N and A5 samples and EDAX image of N and A5.

attaches on the surface of ZNR. With the annealing temperature to 400 °C, it can be observed from Fig. 2b that the surface became much smoother. The above results are basically in agreement with that shown in SEM images. The HRTEM observation (Fig. 2c) reveals that the ultrafine nanoparticles with a

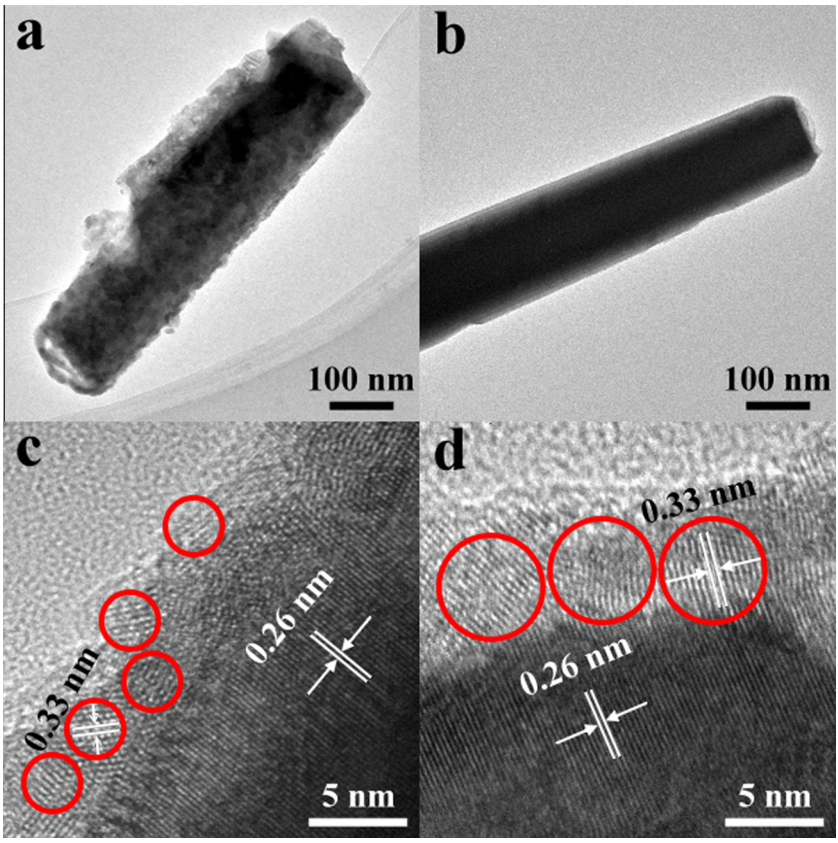

Fig. 2. (a and d) TEM images of N and A4, respectively and (c and d) HRTEM image of N and A4, respectively.

size of 3 nm are deposited on the surfaces of the ZNR for N sample. The well-resolved lattice fringe spacing of ZNR and CdS can be well distinguished to be 0.26 and 0.33 nm, respectively. After the annealing treatment at 400 °C, it can be clearly seen from the HRTEM image (Fig. 2d) of A4 sample that the ZNR is uniformly covered with the larger nanoparticles. The result is basically in agreement with that shown in SEM images. As observed from the HRTEM image in Fig. 2d, nanoparticles grow much bigger (about 5.5 nm) than those before the annealing. And lattice fringe spacing of ZNR and CdS can be distinguished to be 0.26 and 0.33 nm, respectively.

It is well known that surface defect states play important roles in the luminescence properties of nanostructure [23]. Fig. 3a shows the room temperature PL spectrum of the N, A2, A3 and A4 samples, which consists of a dominant UV peak at 379 nm in wavelength and a weak deep level emission (DLE) band in the range of 450–650 nm. Comparing the spectra of N with this recorded on A4, we observe a small red shift (2 nm) in the peak position of the band-edge emission. This result can are attributed to the decrease in the bandgap of CdS QDs. The gradual increase in the overall grain size of CdS QDs with increasing the annealing temperatures represents the decrease in the bandgap of CdS QDs. In order to address this in detail, we propose a possible charge-transfer mechanism, which is schematically illustrated in the inset of Fig. 3. In this modified energy-band diagram it can be seen that the conduction band of CdS with increasing the annealing temperatures would become lower, which is very beneficial to efficiently separate the photo-generated electron–hole pairs and effectively reduce their recombination in each material. So post-annealing treatment can improve the electron transfer in the devices. Thus, post-annealing ZnO photoelectrodes could offer better photovoltaic properties than single N photoelectrode. After the samples were annealed under 200, 300 and 400 °C, the UV emission

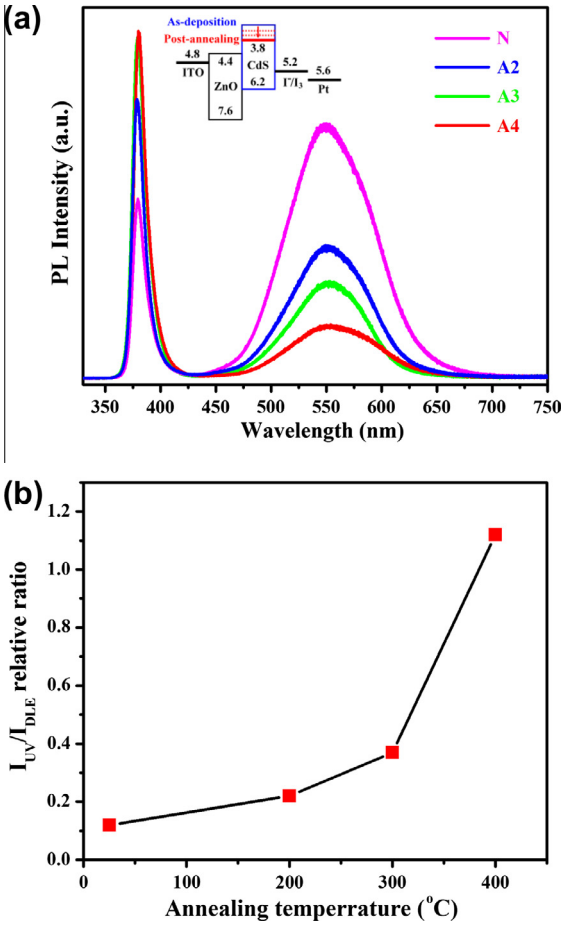

Fig. 3. (a) Room temperature PL spectra of N (pink line), A2 (blue line), A3 (green line) and A4 (red line); (b) I_{UV}/I_{DLE} curve via annealing temperature. The inset shows the arrangement of energy levels and proposed charge-transfer mechanism in post-annealing ZnO photoelectrode. (For interpretation of the references to color in this figure legend, the reader is referred to the web version of this article.)

intensity increased and the deep level emission intensity apparently decreased step by step in comparison with the PL spectrum of the as-deposited sample. The deep level emission band has previously been attributed to several defects in the crystal structure such as O-vacancy [24], Zn-vacancy [25], O-interstitial [26], Zn-interstitial [27], S-vacancy [28], Cd-vacancy [17] and Cd-interstitial [29]. The relative integrated PL intensity ratio between the UV emission (I_{UV}) and deep level emission (I_{DLE}) can be used to characterize the crystallization of all samples [26]. The larger intensity ratio indicates that the samples are in better crystallization, i.e., less deep level defects. The relative integrated PL intensity ratio (I_{UV}/I_{DLE}) as a function of various annealing temperatures were summarized in Fig. 3b. It can be seen that I_{UV}/I_{DLE} value showed a maximum at the annealing temperature of 400 °C. This temperature dependence can be explained from the aspects of the wet chemical growth mechanism and annealing process, respectively. On the one hand, the surfaces of N sample grown with wet chemical method were prone to absorb various kinds of functional groups. According to the chemical reaction in the solution, these functional groups should be related to the elements such as carbon, nitrogen, and hydrogen [30]. These functional groups had a negative influence on the optical properties of N. However after 200 °C annealing, those functional group elements were partially

released from the surfaces of N. During the thermal treatment process at high annealing temperatures of 300 and 400 °C, the absorbed functional group elements were all released from the surfaces of N, as a result, the UV emission intensity is strongly enhanced. On the other hand, as mentioned previously, the DLE band has been attributed to the presence of large amounts of defects, particularly O-vacancy and Zn-vacancy involved complex defects. The less contribution from DLE reflects the less defects existing in the samples, indicating that the thermal treatment make the crystallization of samples turn better with the increase of the annealing temperature. Thus, Fig. 3 proves that A4 sample has the best optical property and crystallization.

As well as we know, the UV–vis absorption spectra of the ZnO/CdS electrodes are strongly dependent on the CdS size and load amount [10,31]. Fig. 4a shows the UV–vis absorption spectra of pure ZNRs, N, A2, A3 and A4. In comparison with the spectrum of ZNRs, we can find that the absorption intensity is obviously enhanced with depositing CdS QDs, especially at the wavelength region of 400–500 nm, which is well corresponding to the emission wavelength region of the CdS QDs. Therefore, we can deduce that the optical absorption properties of the CdS are well preserved after attaching on the ZnO, which result in enhanced light harvesting of the solar energy. To further prove it, the optical band-gap energies (E_g) for the samples have been calculated by the following equation:

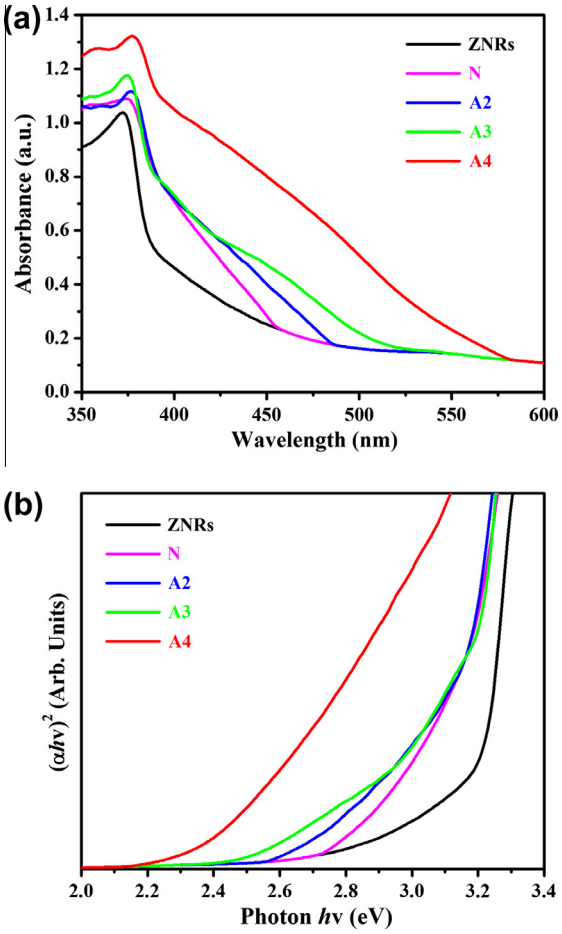

Fig. 4. (a) UV–vis absorption spectra and (b) Tauc plots of bare ZNRs, N, A2, A3 and A4.

$$\alpha(h\nu) = A(h\nu - E_g)^n \tag{1}$$

where α is the absorption coefficient, $h\nu$ is the energy of the incident photon, where A is a constant related to the refractive index and the electron/hole masses, n is 0.5 and 2.0 for a direct and indirect transition semiconductor, respectively [15]. The CdS and ZnO are direct semiconductors so that the n value is 0.5. By employing a Tauc analysis of $(\alpha\, h\, \upsilon)^2$ versus $h\nu$ plotted in Fig. 4b, we extract the E_g to be 3.20, 2.72, 2.64, 2.53 and 2.50 eV for ZNRs, N, A2, A3 and A4, respectively. We observe that the bandgap of the QDs decreases from 2.72 to 2.50 eV with increase the annealing temperature, known as blue shift. The blue shift of the bandgap with increase in dot size is described by the following equation:

$$E_g = E_g^{bulk} + \frac{\hbar^2\pi^2}{2\mu R^2} \tag{2}$$

where E_g^{bulk} is the band gap of bulk CdS, $\hbar = h/2\pi$ (h being Planck's constant), R is the dot size and μ is the effective reduced mass:

$$\mu = \frac{1}{m_o}\left(\frac{1}{m_e^*} + \frac{1}{m_h^*}\right) \tag{3}$$

where m_o, m_e^* (0.2), and m_h^* (0.8) are the mass of the electron, effective mass of electron, and effective mass of hole, respectively [32]. The second term in Eq. (3) represents the kinetic energy [32]. According to Eqs. (2) and (3), the size of CdS QDs can also be calculated, we extract the sizes to be 3.0, 3.5, 4.5 and 5.5 nm for N, A2, A3 and A4, respectively. The sizes of the CdS QDs have a good agreement with the results of TEM. The bandgap of the CdS QDs is found to be varying from 2.72 to 2.50 eV with increase in dot size from 3.0 to 5.5 nm, which agrees with the confinement regime.

Moreover, as shown in Fig. 4, we can also observe the enhancement of absorption intensity and extention of the absorption range for the spectrum of A4 in comparison with the N sample. Herein, we would like to point out that the numbers of SILAR cycles for preparing CdS QDs are same for samples. Plus, we already know that the ZNRs in our case are also completely same, which means they have the almost same length, diameter and even distribution density. Therefore, it is reasonable to propose that the absorption enhancement mainly depends on the increase in grain size of CdS QDs onto ZNRs after the thermal annealing treatments process.

The I–V characteristics of solar cells of N, A2, A3 and A4 under 1.5 AM light illumination have been displayed in Fig. 5. The corresponding performance parameters for each cell are calculated and listed in Table 2, including the short-circuit current density (I_{SC}), the open-circuit voltage (V_{OC}), the fill factor

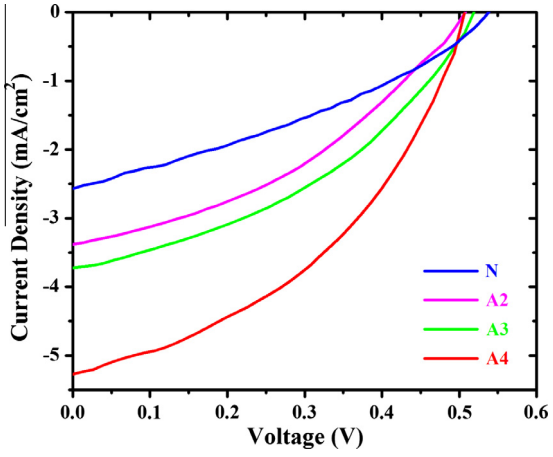

Fig. 5. I–V characteristics of different QDSSCs: N, A2, A3 and A4 photoelectrodes.

Table 2
Photovoltaic parameters obtained from the *I–V* curves of QDSSCs using various photoelectrodes.

Photoelectrodes	I_{SC} (mA/cm^2)	V_{OC} (V)	*FF*	η (%)
N	2.58	0.54	0.335	0.47
A2	3.41	0.51	0.381	0.66
A3	3.74	0.52	0.399	0.78
A4	5.27	0.51	0.421	1.14

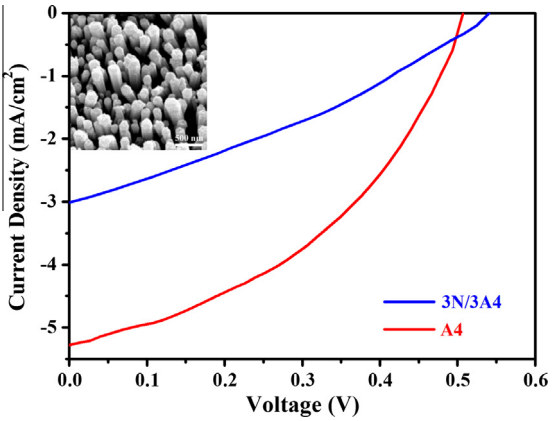

Fig. 6. *I–V* characteristics of different QDSSCs: 3N/3A4 and A4 photoelectrodes. The inset shows the SEM image of 3N/3A4 photoelectrodes.

(*FF*), and the photovoltaic conversion efficiency (η). According to the results in Table 2, the best photovoltaic performance is exhibited by the A4 solar cell, which owns a higher η of 1.14%, I_{SC} of 5.27 mA/cm^2, V_{OC} of 0.51 V and *FF* of 0.421. Compared with the N solar cell, the η of A4 solar cell significantly increases from 0.47% to 1.14%. This up to 143% enhancement of η should be attributed to the increase of both I_{SC} from 2.58 to 5.27 mA/cm^2 and *FF* from 0.335 to 0.421. Normally, the I_{SC} value is mainly dependent on the photocurrent intensity when the cell works. That is to say, in the case of QDSSC, the I_{SC} value should be determined by the absorbance of CdS QDs on the ZnO nanostructures. In comparison with N, the grain size of CdS QDs of A4 is increased, which causes a huge enhancement of absorption range. As a result, more light can be effective absorbed by CdS QDs, which will highly improve the separation efficiency of photo-generated electron–hole pairs in each material and greatly reduce the electron–hole recombination. Therefore, the I_{SC} in A4 cells exhibit a huge increase from 2.58 to 4.76 mA/cm^2. In addition, the slight increase in *FF* is probably due to suppressing charge recombination in the devices since the number of defects is reduced. The *I–V* results further demonstrate that the A4 have advantages over N in light harvesting efficiency, which is consistent with the conclusion obtained from the UV–vis absorption spectra analysis.

In order to investigate the effect of annealing method on the photovoltaic performance of CdS quantum dots sensitized ZNRs solar cells, we have assemble the 3 N/3A4 photoelectrode. The morphology of 3 N/3A4 is nearly as same as the as-deposited sample (N), and the corresponding SEM image can be found in the inset of Fig. 6. Furthermore, *I–V* characteristics for A4 and 3 N/3A4 electrodes were measured. The photovoltaic performance of 3 N/3A electrode is exhibited in Fig. 6, which owns a η of 0.519%, I_{SC} of 3.01 mA/cm^2, V_{OC} of 0.54 V and *FF* of 0.319. Compared with the A4 electrode, the photovoltaic property of the 3 N/3A4 becomes poor. The poor photovoltaic property could be attributed to the poor compact between post-annealed and as-grown CdS QDs layers, which will cause voids in the interface. And it will block the electron transfer, leading to the decline of I_{SC} and *FF*.

4. Conclusions

High density and vertical ZNRs/CdS photoelectrodes have been prepared directly on ITO substrates via a two-step wet chemical method. The annealing temperature and method were crucial to improve the photovoltaic performance of ZNRs/CdS electrodes. The power conversion efficiency (η) of 1.14% was achieved for A4 solar cell. An up to 143% enhancement in η was achieved for A4 solar cell in compare with N solar cell, which can be well explained by two factors. On one hand, the QDs sensitized electrodes with fewer defects can significantly suppressed recombination losses, leading to higher photovoltaic performances. On the other hand, the increase in grain size of CdS QDs onto ZNRs result the absorption intensity and range enhancement after the thermal annealing treatments process. We believe our results can enlighten more researchers to explore effective ways to maximize the power conversion efficiency of photovoltaic device, which will prompt the practical application in the near future, and the results can also further stimulate more theoretical and experimental investigations of the CdS QDs sensitized ZNRs solar cell.

Acknowledgements

The authors acknowledge financial support from National Natural Science Foundation of China (Grant Nos. 61178074 and 61008051), Program for the Development of Science and Technology of Jilin Province (Item Nos. 20110415, 201115219 and 20100113), the Eleventh Five-Year Program for Science and Technology of Education Department of Jilin Province (Item Nos. 20090422, 20110169 and 20110170), the Open Project Program for National Laboratory of Superhard Materials (No. 201004), Program for the Master Students' Scientific and Innovative Research of Jilin Normal University (Item Nos. 201112, 201101 and 201139).

References

[1] T. Bora, H.H. Kyaw, J. Dutta, Electrochim. Acta 68 (2012) 141–145.
[2] W.W. Yu, L. Qu, W. Guo, X. Peng, Chem. Mater. 15 (2003) 2854–2860.
[3] M. Bruchez Jr., M. Moronne, P. Gin, S. Weiss, A.P. Alivisatos, Science 281 (1998) 2013–2016.
[4] G.L. Hornyak, J. Dutta, H.F. Tibbals, A.K. Rao, Introduction to Nanoscience, CRC Press, Taylor & Francis Group, New York, 2008.
[5] A.J. Nozik, Chem. Phys. Lett. 457 (2008) 3–11.
[6] A.J. Nozik, Physica E 14 (2002) 115–120.
[7] Z. Lu, J. Xu, X. Xie, H. Wang, C. Wang, S.-Y. Kwok, T. Wong, H.L. Kwong, I. Bello, C.-S. Lee, S.-T. Lee, W. Zhang, J. Phys. Chem. C 116 (2012) 2656–2661.
[8] W.T. Sun, A. Yu, H.Y. Pan, X.F. Gao, Q. Chen, L.M. Peng, J. Phys. Chem. C 130 (2008) 1124–1125.
[9] G. Zhu, Z. Cheng, T. Lv, L. Pan, Q. Zhao, Z. Sun, Nanoscale 2 (2010) 1229–1232.
[10] C.H. Chang, Y.L. Lee, Appl. Phys. Lett. 91 (2007) 0–0. 053503-1–053503-3.
[11] X.-Y. Yu, J.-Y. Liao, K.-Q. Qiu, D.-B. Kuang, C.-Y. Su, ACS Nano 5 (2011) 9494–9500.
[12] K.S. Leschkies, R. Divakar, J. Basu, E. Enache-Pommer, J.E. Boercker, C.B. Carter, U.R. Kortshagen, D.J. Norris, E.S. Aydil, Nano Lett. 7 (2007) 1793–1798.
[13] Y.J. Lee, D.S. Ruby, D.W. Peters, B.B. McKenzie, J.W.P. Hsu, Nano Lett. 5 (2008) 1501–1505.
[14] L. Tsakalakos, J. Balch, J. Fronheiser, M.Y. Shih, S.F. LeBoeuf, M. Pietrzykowski, P.J. Codella, B.A. Korevaar, O.V. Sulima, J. Rand, A. Davuluru, U.J.J. Rapol, Nanophotonics 1 (2007) 013552.
[15] W. Leea, S.K. Min, V. Dhas, S.B. Ogale, S.-H. Han, Electrochem. Commun. 11 (2009) 103–106.
[16] Y. Zhang, T. Xie, T. Jiang, X. Wei, S. Pang, X. Wang, D.J. Wang, Nanotechnology 20 (2009) 155707–155712.
[17] F. Goto, K. Shirai, M. Ichimura, Sol. Energ. Mater. Sol. C. 50 (1998) 147–153.
[18] K. Shirai, Y. Moriguchi, M. Ichimura, A. Usami, M. Saji, J. Appl. Phys. 35 (1996) 2057–2060.
[19] J. Hiie, T. Dedova, V. Valdna, K. Muska, Thin Solid Films 51 (2006) 443–447.
[20] Y.W. Tang, X.Y. Hu, M.J. Chen, L.J. Luo, B.H. Li, L.Z. Zhang, Electrochim. Acta 54 (2009) 2742–2747.
[21] Q. Jiang, H.X. Shi, M. Zhao, J. Chem. Phys. 111 (1999) 2176–2180.
[22] R. Tena-Zaera, A. Katty, S. Bastide, C. Lévy-Clément, Chem. Mater. 19 (2007) 1626–1632.
[23] S.-M. Liu, F.-Q. Liu, H.-Q. Guo, Z.-H. Zhang, Z.-G. Wang, Solid State Commun. 115 (2000) 615–618.
[24] S. Yamauchi, Y. Goto, T. Hariu, J. Cryst. Growth 260 (2004) 1–6.
[25] X. Yang, G. Du, X. Wang, J. Wang, B. Liu, Y. Zhang, D. Liu, D. Liu, H.C. Ong, S. Yang, J. Cryst. Growth 252 (2003) 275–278.
[26] L.L. Yang, Q.X. Zhao, M. Willander, J.H. Yang, I. Ivanov, J. Appl. Phys. 105 (2009) 0–0. 053503-1–053503-7.
[27] K. Johnston, M.O. Henry, D.M. Cabe, T. Agne, T. Wichert, in: Proceedings of the Second Workshop on SOXESS European Network on ZnO, Caernarfon, Wales, UK, October 2004, pp. 27–30.
[28] A. Blanco, C. López, R. Mayoral, H. Míguez, F. Mesegue, Appl. Phys. Lett. 73 (1998) 1781–1783.
[29] T. Gao, Q. Li, T. Wang, Chem. Mater. 17 (2005) 887–892.
[30] L.L. Yang, Q.X. Zhao, M. Willander, J. Alloys Compd. 469 (2009) 623–629.
[31] P. Ardalan, T.P. Brennan, H.-B.-R. Lee, J.R. Bakke, I.-K. Ding, M.D. McGehee, S.F. Bent, ACS Nano 5 (2011) 1495–1504.
[32] N. Singh, R.M. Mehra, A Kapoor, T. Soga, J. Renew. Sust. Energy Rev. 4 (2012) 0–0. 013110-1–013110-10.